Proceedings of the 13th International Symposium on Experimental Computational Aerothermodynamics of Internal Flows
7–11 May 2017, Okinawa, Japan

ISAIF13-S-0038

Unified classification and characterization of axial turbomachines and propellers

Massyl Lagha, Sébastien Duplaa, Nicolas Binder, Xavier Carbonneau

Université de Toulouse, ISAE-SUPAERO
10 avenue Edouard Belin BP 54032
31055 Toulouse Cedex 4, France
massyl.lagha@isae.fr

Abstract

Reaching the mid/long-term air transport emission reduction goals imposed by both European and American standards impose increasing the propulsive systems' adaptability to various operating conditions, in order to maximize the aircraft overall efficiency all along the flight mission. This implies the enlargement of the design space of propulsive systems such that it can even be operated equally as a compressor or turbine, which leads to rethink the paradigm of designing turbomachines. The continuity in the definition and characterization of different types of turbomachines should be restored which is proposed through this contribution. Analytical relationships allowing to switch between compressor map, propeller map and (ψ, ϕ) map are developed. To minimize the inputs of the maps' conversion relations, a methodology to extract mean flow features from any characterization map is presented, namely the rotor outlet relative flow angle and mean streamline radius. The application of the characterization maps' conversion relations on a turbofan's single-stage axial fan and on a propeller allowed their validation through the physical coherence of the results. The flow features extraction methodology also showed very satisfying results with comparison to experiments. Eventually, the ability of the (ψ, ϕ) formalism as a powerful performance analysis tool for all kind of turbomachines is stressed out, which makes it the best candidate for the unified treatment of turbomachines.
Keywords: turbomachinery, characteristic map, (ψ, ϕ) formalism, performance analysis, fan, propeller

Nomenclature

c_p : specific heat at constant pressure [J/kg/K]
D : rotor diameter [m]
D_s : specific diameter [-]
F : thrust [N]
J : advance ratio [-]
k : rotor axial velocity ratio [-]
$\dot{m}$: mass flow rate [kg/s]
$\boldsymbol{n}$: conventional unit normal vector [-]
N : rotational speed [RPM]
p : pressure [Pa]
P : power [W]
r : rotor radial station [m]
R : gas constant [J/kg/K]
s : rotor outlet-to-inlet cross-section ratio [-]
S : cross-section [m^2]
T : temperature [K]
U : tangential rotational velocity [m/s]
V : absolute velocity [m/s]
$\dot{V}$: flow rate [m^3/s]
$\boldsymbol{z}$: unit axial vector [-]

α : absolute flow angle [rad]
β : relative flow angle [rad]
γ : specific heat ratio [-]
Δh_i : total enthalpy variation [J]
η : efficiency [-]
π_c : total-to-total compression ratio [-]
ρ : density [kg/m^3]
τ : thrust coefficient [-]
τ_c : total-to-total temperature ratio [-]
ϕ : flow coefficient [-]
χ : power coefficient [-]
ψ : work coefficient [-]
ω : rotational speed [rad/s]
ω_s : specific speed [-]

Subscripts
h : hub
i : total quantity
is : isentropic
j : axial station
nom : nominal
opt : optimal
s : shroud
z : axial projection

θ : tangential projection

0: reference (atmosphere)
1: axial rotor inlet station
2: axial rotor outlet station

Introduction

The challenging air transport emission reduction goals imposed by both the European (ACARE) [1] and the American (NASA) [2] standards require development of innovative propulsion technologies. In addition to the increase of efficiency that has to be achieved on propulsive systems, one must consider global optimization of flight operations. This optimization implies that the operating conditions of the propulsive system may have to vary within a wide range during the flight mission. The recent research tendencies head toward the introduction of geometrical variabilities on current propulsive systems [3, 4]. By 2050, the IATA [5] demonstrate that emission reduction goals cannot be achieved without shifting research towards disruptive technologies such as distributed propulsion.

The purpose of introducing geometrical variabilities or distributing propulsion is to propose a larger design space in order to increase the propulsive systems' adaptability to various operating conditions. This would allow considering maximization of aircraft overall efficiency all along the flight mission. In case of distributed propulsion, it would make it possible to partially recover power through the windmilling of a limited number of propulsive modules during descent phase.

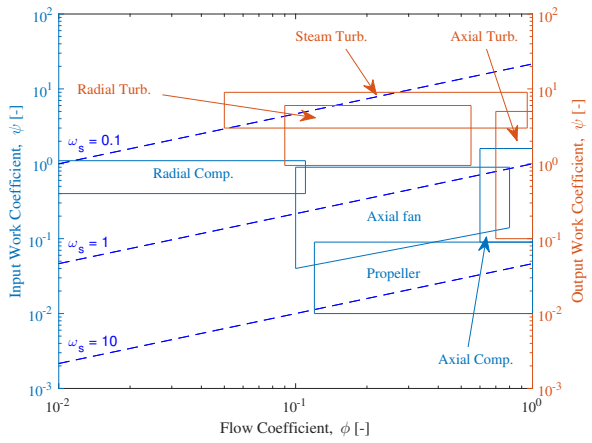

Figure 1 Turbomachines design windows (adapted from Japikse & Baines [6])

In order to enlarge design space and to propose dual operating design (compressor-turbine), one must reconsider the multiple turbomachines' classifications and go back to their most general definition, namely: "a mechanical device exchanging work with a continuous fluid flow through one or multiple rotors". This vision is necessary as the turbomachines' community has been divided since its early birth due to the intimate link between the field of turbomachinery and engineering companies. Theses companies make designs more specific and less public, which prevent development of a unified vision and tools for turbomachines' analysis. One of the most striking examples that illustrates this division is the very distinct treatment that is made for propellers that are considered as a specialized field of external flows aerodynamics while all other turbomachines are related to internal flows aerodynamics. For this reason, propellers are often not even considered as turbomachines whereas they perfectly match the abovementioned definition. The main differences between propellers and the other turbomachines lies in the lower solidity and work input of propellers which allow their treatment through more classical fluid mechanics tools that are usually attributed to external flows aerodynamics [7]. Still, it is not a sufficient reason to break continuity between propellers and the rest of turbomachines.

In fact, as it can be depicted in many excellent reference literature [8, 9], turbomachines are firstly classified into different types and then treated independently using different design and analysis tools. Each type is also restricted to a precise specification window as presented by Japikse and Baines [6] (cf. figure 1).

This compartmentalization is mainly due to the work of Cordier [10] further developed by Balje [11] aiming to correlate non-dimensional numbers (specific speed ω_s and specific diameter D_s) to the optimal turbomachine's geometry. Those non-dimensional numbers, as defined by Balje are:

$$\omega_s = \omega \frac{(\dot{V})^{1/2}}{(\Delta h_i)^{3/4}} \quad (1)$$

$$D_s = D \frac{(\Delta h_i)^{1/4}}{(\dot{V})^{1/2}} \quad (2)$$

Cordier and Balje computed these numbers from measurements of several turbomachines working on their best efficiency point. Plotting these results shows that the best machines lie in a relatively narrow band, so called Cordier or Balje line (cf. figure 2, note that here the definitions of the dimensionless numbers differ slightly from that of equations (1) and (2) : $\sigma = 2^{-3/4}\pi^{-1/2}\omega_s$ and $\delta = 2^{-3/4}\pi^{1/2}D_s$). It has to be pointed out that it is a mean empirical line only true in the statistical sense, even if this approach and the resulting classification still a very useful tool for engineers to help guiding the turbomachinery's design from a limited number of inputs. That is to say, it is possible to design a high-efficiency machine far from the Cordier line, especially axial machines as the scatter of points is quite wide in the axial region.

Casey et al. [12] also outlined several important points in their analysis of the Cordier diagram. As a matter of fact, the dimensionless parameters shown in equations (1) and (2) are incompressible by nature. Therefore, the influence of the relative inlet Mach number is not taken into account in the Cordier line. Moreover, the exact location of this line may be strongly driven by the blade geometry, namely the number of blades, the solidity, the pitch angle, the tip clearance and the hub to shroud ratio. Epple et

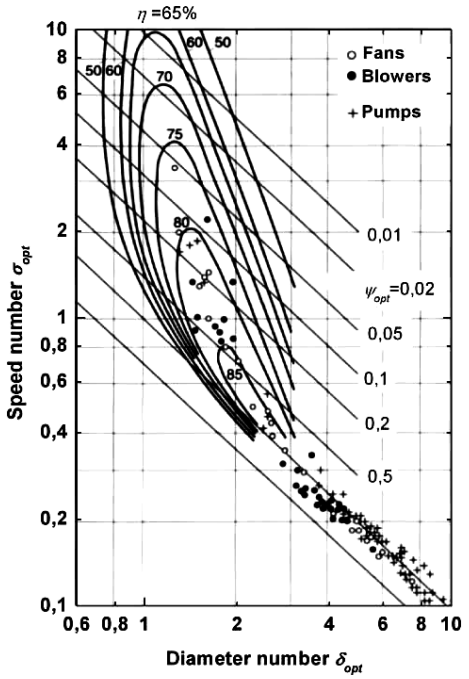

Figure 2 Cordier diagram [10]

al. [13] derived theoretical expressions for the Cordier line where the influence of the pitch angle and hub to shroud ratio appears clearly and demonstrate the effect of these parameters on the scatter of points on the Cordier diagram. Hence, one could easily consider that the Cordier line and the resulting classification are of less relevance when it comes to design variable geometry or dual operating turbomachines.

A more universal design approach is then needed to handle these new specifications. Lewis [14] extensively developed a design method based on dimensionless performance variables, namely the work coefficient ψ and the flow coefficient ϕ defined as:

$$\psi = \frac{\Delta h_i}{(\omega D)^2} \tag{3}$$

$$\phi = \frac{\dot{m}}{\rho_{i_1} \omega D^3} \tag{4}$$

As these parameters and their incompressible derivatives are naturally derived from the dimensional analysis, they often appear in works treating of the unification of turbomachines. For instance, the (ψ, ϕ) diagram appears in the four-quadrant approaches developed by Knapp et al. [15] and after that by Turner and Sparkes [16] that help exploring all functioning points of a turbomachine (compressor, turbine, dissipation...) whether the flow discharge is positive (design direction) or inversed, and in both rotational directions of the rotors. Gill et al. [17] also used the (ψ, ϕ) diagram through the four-quadrant approach to analyze aerodynamics of compressors under windmilling operation. Binder et al. [18, 19] have been extensively using the (ψ, ϕ) formalism to predict variable geometry turbine performances and also to treat fan windmilling.

Scope

The (ψ, ϕ) diagram seems to emerge from the turbomachines' literature when it comes to treat the design of the machine in a unified manner as depicted by Lewis [14]. In the other hand, this formalism appears as a powerful performance analysis tool regardless of the turbomachine's function or operating point as shown by Gill et al. [17] and Binder et al. [18, 19].

Yet, each "type" of turbomachine still, in usual practices of the community, characterized by its own characteristic map that is limited to the narrow windows depicted in figure 1 : The $(H, \dot{V})$ map for hydrodynamic turbomachines, the propeller characteristic map for free or ducted propellers, the $(\pi, \dot{m})$ for compressors and turbines. Therefore, in order to analyze the performances of the current turbomachines in the light of the more unified characterization that represents the (ψ, ϕ) diagram, it is compulsory to develop relationships between the above mentioned characteristic maps and the (ψ, ϕ) diagram. The establishment of these relationships represents the main objective of this paper.

Besides, a methodology to extract, from the (ψ, ϕ) characterization, the turbomachine's flow angles and the meridional plane mean-streamline will be presented. This will allow minimization of the needed inputs for the characteristic maps' conversion relations, hence strengthen their generalization to all turbomachines.

Eventually, the characteristic map conversion and the flow features extraction will be applied to a turbofan's fan stage and also to a propeller which will allow the validation of the developed methods through physical analyses and comparison to experiments. This will also stress the powerful potential of the (ψ, ϕ) formalism as a performance analysis tool.

Geometric and functioning hypotheses

The focus in this paper will be on single-stage axial compressors and propellers, but the method developed could also be applied to single-stage axial turbines.

Steady, axisymmetric, adiabatic flow of inviscid perfect gas will be considered in the following developments. Furthermore, a mean-line treatment will be made, which means that the layer flow located at a reference radius will be considered as representative of the mean flow in the turbomachine. Therefore, all quantities will be computed for the reference radius defined as [20]:

$$r_j = \sqrt{\frac{r_{s_j}^2 + r_{h_j}^2}{2}} \tag{5}$$

Where subscript s refers to the shroud, h refers to the hub and j refers to the axial location of a given plane (1 for the rotor inlet plane and 2 for the rotor outlet plane).

Regarding the blade-to-blade plane, all angles and velocities of interest are depicted in figure 3. In addition to this, a mean rotor cross-section will be defined as:

$$S_{mean} = \frac{S_1 + S_2}{2} \tag{6}$$

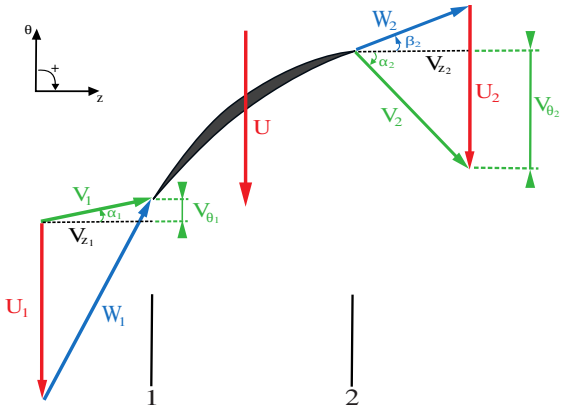

Figure 3 Velocity triangles definition

And only on this section, a linear evolution of density and axial velocity will be assumed which leads to:

$$V_{z_{mean}} = \frac{V_{z_1} + V_{z_2}}{2} \quad (7)$$

$$\rho_{mean} = \frac{\rho_1 + \rho_2}{2} \quad (8)$$

Characterization maps' definitions

The compressors are often characterized using multiple curves depicting the evolution of the compression ratio and the isentropic efficiency versus corrected mass flow at iso-rotational speed. It will be further referred to this characterization as (π_c, MFP, η_{is}) where MFP is the acronym for Mass Flow Parameter.

$$\pi_c = \frac{p_{i_2}}{p_{i_1}} \text{ (compression ratio)} \quad (9)$$

$$MFP = \frac{\dot{m}}{S_1 p_{i_1}} \sqrt{\frac{T_{i_1} R}{\gamma}} \quad (10)$$

$$\eta_{is} = \frac{\pi_c^{\frac{\gamma-1}{\gamma}} - 1}{\tau_c - 1} \text{ (isentropic efficiency)} \quad (11)$$

It must be stressed here that the rotational speed does not appear in the (π_c, MFP, η_{is}) definition equations. This explains the iso-rotational speed feature of the characteritics in this map and also the necessity of multiple curves to depict the whole operating range of the machine.

The propeller chart characterizes the functioning of a propeller through several curves depicting the evolution of the thrust coefficient and the power coefficient versus the advance ratio at iso-pitch angle. It will be further referred to this characterization as (τ, J, χ).

$$\tau = \frac{F}{\rho_{i_1} U_1^2 S_{mean}} \text{ (thrust coefficient)} \quad (12)$$

$$J = \frac{V_{z_1}}{U_1} \text{ (advance ratio)} \quad (13)$$

$$\chi = \frac{P}{\rho_{i_1} U_1^3 S_{mean}} \text{ (power coefficient)} \quad (14)$$

Regarding **the (ψ, ϕ) formalism**, it depicts the evolution of the work coefficient and the isentropic efficiency versus the flow coefficient at iso-compression ratio. It is then more relevant to refer to this characterization as (ψ, ϕ, η_{is}). Moreover the definition further used might slightly differ from that presented in equations (3) and (4) to be replaced by:

$$\psi = \frac{\Delta h_i}{U_1^2} \quad (15)$$

$$\phi = \frac{\dot{m}}{\rho_{i_1} U_1 S_1} \quad (16)$$

While the isentropic efficiency η_{is} still defined as in equation (11).

Even if the characterizations previously presented seem different, they share the same physical basis, which is to be derived from the dimensional analysis of a turbomachine. Indeed, the mass flow parameter at iso-rotational speed, the advance ratio or the flow coefficient reflect the rotor inlet relative flow angle, which is with analogy to an airfoil incidence angle, one of the first order driving parameter of the functioning mechanism of the turbomachine. Also, the compression ratio, the thrust coefficient or the work coefficient reflect the quantity of interest that is derived from the machine while the isentropic efficiencies reflect the amount of losses as a turbomachine not only exchanges work with the flow but produces entropy too.

The proximity of these characterizations is exploited in the following developments to relate the different dimensionless parameters by pairs and then create the bridges between the multiple maps.

(π_c, MFP, η_{is}) and (ψ, ϕ, η_{is}) maps' relationship

Now that all characteristic maps definitions had been set, it appears that passing from the (π_c, MFP, η_{is}) map to the (ψ, ϕ, η_{is}) map is kind of straight forward and well-known. Indeed, having the compressor conventional map and predesign data of geometry and functioning ([*i*]the rotor inlet radii at hub and shroud; [*ii*]total pressure, temperature and the flow pre-swirl angle at inlet; [*iii*]the fluid specific heat ratio) it is possible to express the work coefficient and the flow coefficient as follows:

$$\psi = \frac{c_p(T_{i_2} - T_{i_1})}{U_1^2} = \frac{\gamma R}{\gamma - 1} \frac{T_{i_1}}{U_1^2} (\tau_c - 1) \quad (17)$$

$$\phi = \frac{V_{z_1} \rho_1}{U_1 \rho_{i_1}} \quad (18)$$

Where the axial velocity V_{z_1} and the static-to-total density ratio ρ_1/ρ_{i_1} at the rotor inlet can be expressed as functions solely depending of the rotor inlet axial Mach number M_{z_1}, through the isentropic flow relations and the Mach number and velocity triangle definitions:

$$\frac{\rho_1}{\rho_{i_1}} = \left[1 + \frac{\gamma - 1}{2} M_{z_1}^2 (1 + \tan^2 \alpha_1)\right]^{-\frac{1}{\gamma - 1}} \quad (19)$$

$$V_{z_1} = \frac{M_{z_1}}{\sqrt{1 + \frac{\gamma - 1}{2} M_{z_1}^2}} \sqrt{\gamma R T_{i_1}} \quad (20)$$

Eventually the rotor inlet Mach number can be computed using a basic Newton-Raphson method on the following mass conservation equation:

$$MFP = M_{z_1}\left(1+\frac{\gamma-1}{2}M_{z_1}^2\right)^{-\frac{\gamma+1}{2(\gamma-1)}} \quad (21)$$

Inversely, by starting from a (ψ, ϕ, η_{is}) map and predesign data of geometry and functioning, it is possible to compute the (π_c, MFP, η_{is}) map for a given rotational speed using equations (17) to (21).

(τ, J, χ) and (ψ, ϕ, η_{is}) maps' relationship

The relationship between the (τ, J, χ) map and the (ψ, ϕ, η_{is}) map is more complex than the one previously established. It should then be helpful to first convert the propeller map to a (π_c, MFP, η_{is}) map and then pass it to the (ψ, ϕ, η_{is}) map using the previous method.

In order to establish the relation between the (π_c, MFP, η_{is}) map and the (τ, J, χ) map, one must first derive the thrust of the turbomachine from the momentum balance equation:

$$F = \int_{\partial S}\left[(p-p_0)\boldsymbol{n}+\rho(\boldsymbol{V}\cdot\boldsymbol{n})\boldsymbol{V}\right]dS\cdot\boldsymbol{z} \quad (22)$$

Then by neglecting the conicality of the system, it is possible to approximate the rotor inlet and outlet sections by the mean rotor cross-section introduced in the equation (6), giving:

$$F \approx S_{mean}\Delta p + \dot{m}\Delta V_z \quad (23)$$

Where $\Delta p = p_2 - p_1$ and $\Delta V_z = V_{z_2} - V_{z_1}$ represents the rotor outlet-inlet pressure and axial velocity variation. This leads, by applying the mass conservation between the rotor inlet, outlet and mean cross-sections and by introducing the equations (6), (7), (8) and (13), to:

$$\tau = \left[\frac{\Delta p}{\rho_{i_1}V_{z_1}^2} + \frac{\rho_1}{4\rho_{i_1}}(k^2-1)\left(\frac{1}{ks}+1\right)\right]J^2 \quad (24)$$

With $k = {}^{V_{z_2}}/_{V_{z_1}}$ and $s = {}^{S_2}/_{S_1}$ are the rotor outlet-to-inlet axial velocity and cross-section ratios respectively.

In order to relate the power coefficient χ to the compressor map parameters, one must consider the energy conservation:

$$P = \dot{m}\Delta h_i = \dot{m}\frac{\gamma R}{\gamma-1}T_{i_1}(\tau_c - 1) \quad (25)$$

Then by applying the same relations that allow passing from the equation (23) to (24) and by using the Mach number definition:

$$\chi = \frac{k+1}{\gamma-1}\frac{\rho_1}{4\rho_{i_1}}\left(\frac{1}{ks}+1\right) \times (\tau_c-1)\left(\frac{1}{M_{z_1}^2}+\frac{\gamma-1}{2}\right)J^3 \quad (26)$$

Equations (13), (24) and (26) show that if one knows the (π_c, MFP, η_{is}) map, the rotor outlet section and predesign data of geometry and functioning, it is possible to compute the (τ, J, χ) map. In fact, the advance ratio J can be simply derived by using equations (20) and (21). After that, the determination of the power coefficient χ only needs the computation of the axial velocity ratio k that can be expressed, using the isentropic flow relations and the Mach number definition, as follows:

$$k = \frac{M_{z_2}}{M_{z_1}}\sqrt{\tau_c\frac{1+\frac{\gamma-1}{2}M_{z_1}^2}{1+\frac{\gamma-1}{2}M_{z_2}^2}} \quad (27)$$

Where the rotor outlet axial Mach number is given by applying a Newton-Raphson method on the following mass conservation equation:

$$MFP\frac{\sqrt{\tau_c}}{\pi_c s} = M_{z_2}\left(1+\frac{\gamma-1}{2}M_{z_2}^2\right)^{-\frac{\gamma+1}{2(\gamma-1)}} \quad (28)$$

Still, it is necessary to compute the static pressure variation Δp to obtain the thrust coefficient τ. This pressure variation can be calculated by using the isentropic flow equations and some basic trigonometric laws applied on the velocity triangles:

$$p_1 = p_{i_1}\left(1+\frac{\gamma-1}{2}M_{z_1}^2(1+\tan^2\alpha_1)\right)^{-\frac{\gamma}{\gamma-1}} \quad (29)$$

$$p_2 = \pi_c p_{i_1}\left[1+\frac{\gamma-1}{2}M_{z_2}^2 \times \left(1+(\frac{r_2}{r_1}\frac{1}{Jk}+\tan\beta_2)^2\right)\right]^{-\frac{\gamma}{\gamma-1}} \quad (30)$$

Inversely, if one starts from a (τ, J, χ) map, the rotor outlet section and predesign data of geometry and functioning, it is possible to compute the (π_c, MFP, η_{is}) map using the previous equations.

Flow angles and the meridional plane mean-streamline extraction

Although some flow features as the relative outlet flow angle β_2 and the mean-streamline rotor outlet radius r_2 are present in the equation (30), they are not mentioned as inputs to pass from a (π_c, MFP, η_{is}) map to a (τ, J, χ) map and vice versa. This is due to the fact that these quantities can be analytically extracted from the (ψ, ϕ, η_{is}) map. Indeed, it is possible to relate the work coefficient to the flow coefficient by using the Euler theorem and the velocity triangles definitions as follows:

$$\psi = \frac{\Delta h_i}{U_1^2} = \frac{U_2V_{\theta_2} - U_1V_{\theta_1}}{U_1^2} \quad (31)$$

Which leads, after some manipulations, to:

$$\psi = \left(\frac{r_2}{r_1}\right)^2 + \frac{\rho_{i_1}}{\rho_1}\left(\frac{r_2}{r_1}k\tan\beta_2 - \tan\alpha_1\right)\phi \quad (32)$$

It must be stressed here that the equation (32) is not a linear function of the flow coefficient ϕ since the rotor outlet-to-inlet axial velocity ratio k will necessarily vary with ϕ. The reason is the dependence of k mainly on the compression ratio and the isentropic efficiency as depicted by the equations (27) and (28). Moreover, one can notice that the factor k will be close to unit in the case of incompressible flow and neglected conicality of the machine, due to mass conservation. The distance of the factor k from unit can therefore be considered as a measure of the incursion of the turbomachine in the compressible domain.

Besides, the rotor outlet relative flow angle β_2 can no more be stated constant if one consider the deviation of the flow from the rotor outlet blade angle. This deviation angle is at iso-geometry of the machine a function of the incidence angle on the blade and Mach number as stated by Carter [21]. This deviation angle can be reformulated as a function of the isentropic efficiency and the k factor, as the former is at first order driven by the incidence angle and the later a function of the variation of the Mach number through the machine.

The non-linearity of the equation (32) can then be related, on the one hand to the compressibility of the flow through the machine and on the other hand to the entropic nature of the flow. The rotor outlet-to-inlet axial velocity ratio k and the isentropic efficiency η_{is} allow to gauge those features of the flow. Consequently, if one consider the optimum operating range of relatively low pressure turbomachines, the variation of k and η_{is} will be small enough to consider the equation (32) as linear.

Moreover, the work coefficient and the flow coefficient can be computed by using exclusively inputs from the rotor inlet plane as shown by the equations (17) to (21). Consequently, the linear fitting of the resulting coefficients and the equation (32) make it possible to extract the values of r_2 and β_2 starting from any characterization map and the limited number of inputs previously enumerated.

Analysis of a converted compressor map

In order to test the coherence of the presented method, it had been applied on the characterization map of the DGEN-380 fan. The DGEN-380 is a turbofan designed to deliver a 2500N thrust and intended to equip personal light jets (4-5 passengers). A complete instrumented test bench of this engine is available at the Department of Aerodynamics, Energetics and Propulsion of ISAE-SUPAERO [22]. The figure 4 sums up roughly the architecture of this engine.

The complete fan stage (rotor and stator) had been simulated to produce the conventional (π_c, MFP, η_{is}) map depicted in figure 5. The numerical domain starts upstream of the spinner and ends right upstream of the splitter duct. A mixing plane is located between the rotor and the stator. The geometry of the fan includes the hub fillet and the tip clearance gap.

The numerical domain is discretized with a multi-block structured mesh generated with Numeca's Autogrid 5^{TM},

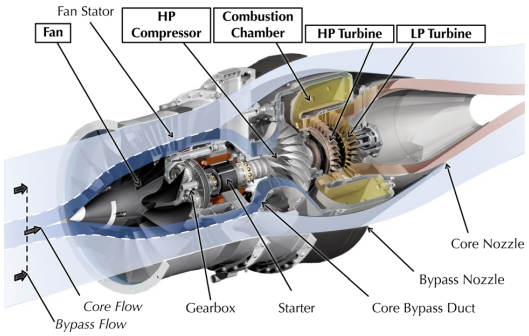

Figure 4 DGEN-380 architecture

consisting of O-type blocks around the blades, and H-type blocks to fill the passage. The first cell at the wall has a size of 10 μm, ensuring a value of $\Delta y_w^+ \sim 1.4$ over the blades for all the simulations. The expansion ratio across the boundary layer mesh is about 10%. Non-matching connections are used on periodic faces to facilitate the generation of a high-orthogonality mesh. Overall, the mesh is comprised of about 7.9 million points with 3.5 million points in the rotor and 4.4 million points in the stator.

The simulations are performed with the Euranus solver of the Fine/Turbo^{TM} package of Numeca. For steady problems, the Reynolds-averaged Navier-Stokes equations (RANS) in the rotating frame are solved with a pseudo-time-marching method. Time integration is ensured by a four-stage Runge-Kutta scheme with implicit residual smoothing. Local time stepping and a three-level multigrid technique are used to accelerate convergence to the steady state. The discretization in space is based on a cell-centered finite-volume approach. Convective fluxes are determined by a second-order centered scheme with added artificial dissipation of the Jameson type. Viscous fluxes are centered. The mixing plane interface is treated with a conservative coupling by pitchwise rows. Turbulence closure is provided by the one-equation model of Spalart and Allmaras.

At the inlet of the numerical domain, radial profiles are imposed according to the experimental measurements. At outlet, static pressure is imposed with a radial equilibrium condition. For further details about the computational simulation, one can refer to the work of Dufour et al. [23].

It is interesting to stress here the relatively small compression ratios of this fan in comparison with the conventional aircraft engines' fans. This is due to the smaller diameter of the engine that makes the fan operating in the subsonic domain at all radial stations.

Before applying the map modification, it is crucial to confirm that the starting map is in the scope of the hypotheses made initially. In fact, the presented equations apply only on the rotor of the turbomachine. Before going any further, it must be confirmed that the influence of the stator on the characterization map is negligible. To do so, one must make sure that the losses in the stator are negligible with comparison to the work input of the rotor. Yet these losses are known to rise as the system gets into the choked functioning and make the compression ratio and

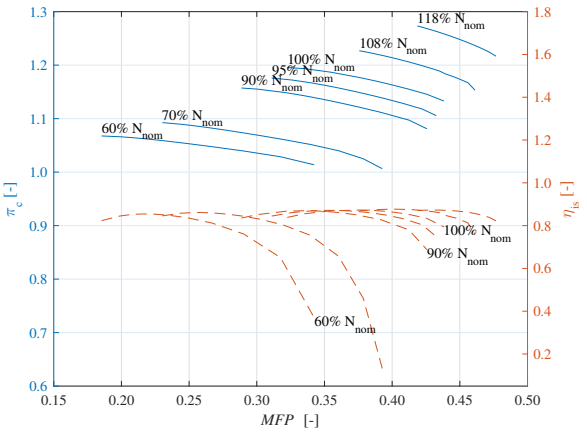

Figure 5 DGEN-380 (π_c, MFP, η_{is}) map

the isentropic efficiency plummet. This phenomenon had been observed in the performed numerical simulations and is caused by the formation of shock waves in the stator when the flow is choked. These shock waves raise the losses of the stator in terms of total pressure decrease and make them of the same order of magnitude as the rotor compression ratio. Consequently, by treating exclusively the unchoked part of the compressor map, one can assume the validity of the previously exposed developments as the stator influence on the map can be neglected.

First, the unchoked part of the compressor map of the DGEN-380 fan had been converted into a (ψ, ϕ, η_{is}) map. The results are provided in the figure 6. The resulting flow and work coefficients are of the same order of magnitude comparing with similar installations [19].

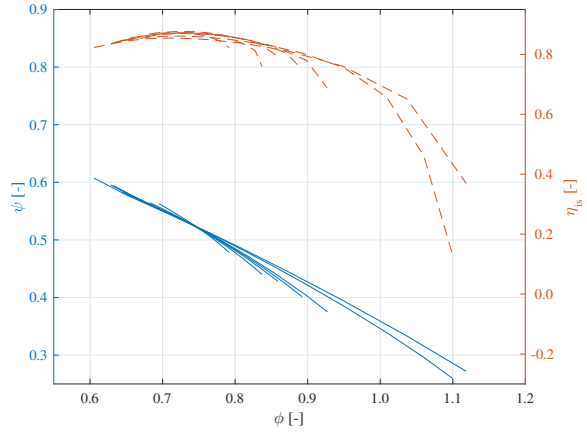

Figure 6 DGEN-380 (ψ, ϕ, η_{is}) map

It can be noticed that both ψ and η_{is} characteristics collapses approximatively on the same line as expected. As a matter of fact, this gives the conversion methodology a first level of validation as the uniqueness of these characteristics is predicted by the dimensional analysis theory. As stated before, in the conventional compressor maps, the rotational speed is an independent parameter that is not taken into account in the dimensionless groups as shown by the equations (9) to (11), which leads to an isolated characteristic for each rotational speed. Actually, in opposition to the (π_c, MFP, η_{is}) map, the (ψ, ϕ, η_{is}) map is the natural result of the dimensional analysis where all independent variables driving the turbomachine's functioning are taken into account except the compressibility and the viscosity. The small discrepancies observed at high flow coefficient are due to these two later parameters that can be represented respectively by the variations of the rotor outlet-to-inlet axial velocity ratio k and the isentropic efficiency η_{is}.

Furthermore, the quasi-superposition of the characteristics in the (ψ, ϕ, η_{is}) map reflects an operating similarity of the fan at all rotational speeds, which is commonly observed for incompressible hydrodynamic turbomachines. However, the relative tip Mach number of the fan at high rotational speed almost reaches unit value which is, in usual practices of the community, considered as indicating the incursion in the compressible operating domain. Consequently, the relative tip Mach number may not be the relevant parameter to depict the incursion in the compressible domain in the mean-streamline treatment of the turbomachine. The compression ratio and the isentropic efficiency and therefore the factor k seems more relevant to characterize this incursion since they alter the linearity of the equation (32) as stated in the previous section. The table 1 shows that the mean k factor over each iso-rotational speed is close to unit. It is then possible to conclude that the functioning of an unchoked turbomachine can be approximated by an incompressible mean-streamline approach while the variation of the axial velocity through the rotor stays small, even if the relative tip Mach number is high.

Table 1 DGEN-380 rotor mean outlet-to-inlet axial velocity ratio k

Rotational speed [$\%N_{nom}$]	k
60	1.0712
70	1.0631
90	1.0165
95	1.0012
100	0.9860
108	0.9612
118	0.9245

Given that the (ψ, ϕ, η_{is}) map of the DGEN-380 had been computed using the developed method, it make it possible to extract the values of the rotor outlet relative flow angle β_2 and mean-streamline radius r_2. It is important to stress here that the conversion of the compressor map had been performed at iso-rotational speed. That is to say that the characteristics in the (ψ, ϕ, η_{is}) map depict the evolution of the work coefficient and the isentropic efficiency versus the flow coefficient at iso-rotational speed and not at iso-compression ratio. Strictly speaking, the resulting characteristics don't represent a valid (ψ, ϕ, η_{is}) map. However, the collapse of the characteristics into a single line due to the little variation of the k factor makes the difference between the iso-rotational speed and the iso-

compression ratio characteristics negligible. Still, the iso-rotational treatment of the map conversion allows building characteristics with a higher number of points which makes the fitting operation far more robust. It is therefore possible to postulate that the higher quality of the fitting operation compensate the physical error introduced by the iso-rotational speed treatment. This is the reason why this little deviation seems acceptable.

The obtained results are very satisfying and give a second level of validation to the method. Actually, the computed flow angle gives β_2 =-32.8^o at the design point of the fan while experiment gives β_2^{exp} =-29^o [22], that is to say a relative error of 13% which is very conclusive for such analytical method. Moreover, the computed mean-streamline radius gives r_2 =136mm that is the exact value obtained by using the equation (5), which confirms the relevance of this definition of the mean-streamline.

The computation of the values of the rotor outlet relative flow angle and mean-streamline radius makes it possible to convert the initial (π_c, MFP, η_{is}) map to (τ, J, χ) map by applying the presented method. The obtained results are depicted in the figure 7. One can notice that the resulting thrust coefficient, power coefficient and advance ratio are of the same order of magnitude comparing with propellers producing equivalent thrust (i.e. the 568F propeller driven by the PW-127M engine that equips the ATR-72 [24]).

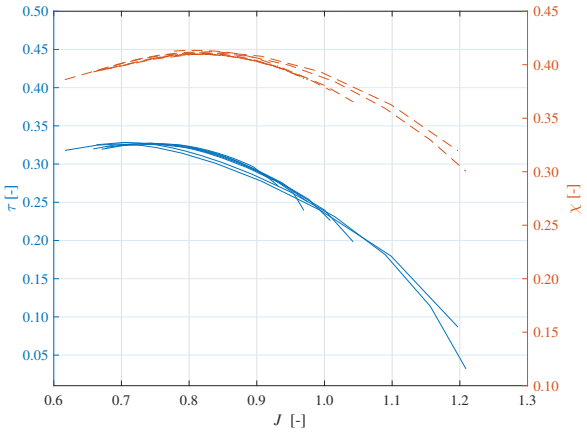

Figure 7 DGEN-380 (τ, J, χ) map

Similarly to the observation made on the (ψ, ϕ, η_{is}) map, the characteristics on the propeller map collapse into a single line. This result confirms the validity of the developed method since the (τ, J, χ) map takes also into account all the independent variables driving the turbomachine's functioning except the compressibility and the viscosity. Also, this quasi-superposition of the characteristics confirms the small influence of the compressibility on the global functioning parameters of the fan as analyzed before.

Analysis of a converted propeller map

In the previous section, the developed methodology had been tested by converting a compressor map into (ψ, ϕ, η_{is}) map and propeller map. Still, it is interesting to test the bijectivity of the method by starting from a propeller map. To do so, the wind tunnel test results of the 3.048m diameter four blade Clark-Y 5868-9 propeller performed by Hartman and Biermann [25] had been taken as reference propeller map. Hartman and Biermann produced the complete propeller characterization for multiple blade pitch angles and presented it in a classical fashion through a (τ, J, χ) map that is depicted in figure 8.

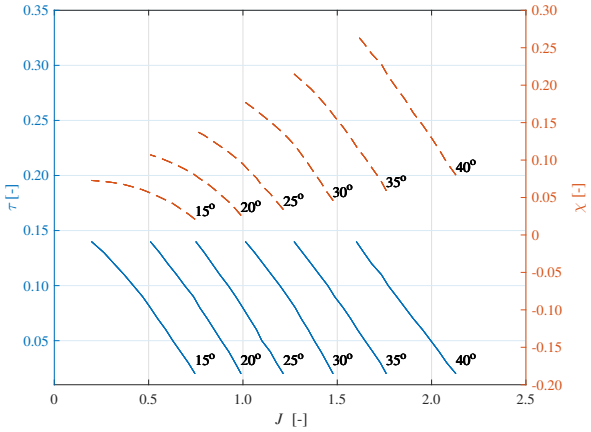

Figure 8 Clark-Y 5868-9 (τ, J, χ) map

The conversion methodology had been applied to each iso-pitch angle characteristic and the results are depicted in the figure 9. Here, the mean k factor value on each curve is about 0.98 which reflects the incompressible aspect of the flow through the propeller. That allows admitting the validity of the map conversion along iso-pitch angle curves.

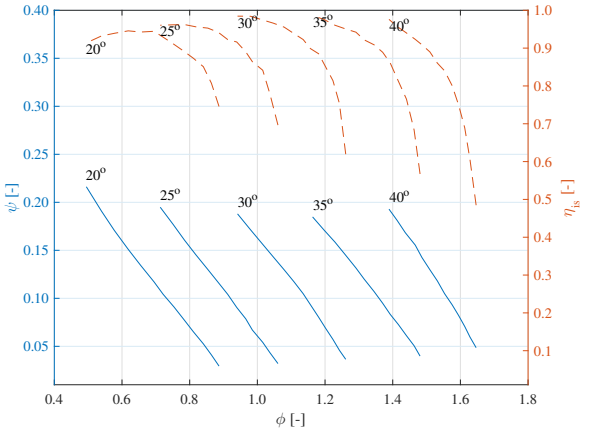

Figure 9 Clark-Y 5868-9 (ψ, ϕ, η_{is}) map

First it can be noticed that the propeller iso-pitch angle characteristics in the (ψ, ϕ, η_{is}) map are linear as expected by the theoretical derivation shown in equation (32). In this case, the uniqueness of the characteristics is not observed due to the variation of the pitch angle that represents an independent variable not taken into account in the dimensional analysis performed to build the dimensionless

groups. Also, even if the resulting characteristics seem to be parallel, it is actually not the case. The table 2 sums up the linear fitting coefficients of each characteristic and shows that the characteristics are not parallel.

Table 2 Clark-Y 5868-9 (ψ, ϕ, η_{is}) map linear fitting coefficients as $\psi = a\phi + b$

Pitch angle	a	b
20^o	-0.4635	0.4404
25^o	-0.4657	0.5272
30^o	-0.4740	0.6386
35^o	-0.4566	0.7192
40^o	-0.5601	0.9741

It is interesting to focus on the coefficient b that depicts, according to the equation (32), the squared rotor outlet-to-inlet mean-streamline radius ratio. It takes under unit values which can seem unexpected. Indeed, in compressors for which the (ψ, ϕ, η_{is}) map is more often used, the convergence of the cross-section is a design commonly admitted as it allows stable operating of the machine by maintaining a quasi-constant axial velocity. This feature, in addition to the casing that confines the flow, makes the mean-streamline increase radius which leads to a rotor outlet-to-inlet mean-streamline radius ratio over unit. However, in the case of the studied propeller, there is neither cross-section evolution nor casing which makes the stream tube's geometry defining the flow through the propeller function of its operating parameters. As a matter of fact, this stream tube has a convergent form due to the propeller work input [26]. This is the reason why the computed rotor outlet-to-inlet mean-streamline radius ratio takes values under unit. Moreover, as depicted in the reference literature [26], the convergence of the stream tube decreases with the increase of the advance ratio. This phenomenon can also be observed in the table 2 through the evolution of the value of the rotor outlet-to-inlet mean-streamline radius ratio which tends to unit when the pitch angle and therefore the related advance ratio increase (cf. figure 8).

These observations demonstrate that the mean-streamline radius definition given by the equation (5) is not relevant for the treatment of free propellers; one better prefers in that case simply the rotor radius as it is representative of the stream tube radius at upstream far field.

Eventually, the rotor outlet relative flow angle β_2 had been extracted using the developed method and had been compared to the blade pitch angles considering that this angle reflects the mean blade profile trailing edge angle. The table 3 sums up the obtained results. It is important to clarify that these results are not meant to be quantitative as more experimental data are needed to make a proper comparison. The objective here is to stress the ability of the (ψ, ϕ, η_{is}) formalism to highlight off-design functioning.

As expected, except for the 30^o pitch angle which is the design pitch of the propeller, the values of the deviation angle are quite high. Indeed, the low solidity of the propellers due to their little number of blades make these machines far more sensitive to flow detachments when operating at off-design points.

Table 3 Flow and blade angle comparison

Pitch angle	Flow angle	Deviation angle
20^o	33.8^o	13.8^o
25^o	30.9^o	5.9^o
30^o	28.2^o	1.8^o
35^o	25.6^o	9.4^o
40^o	25.4^o	14.6^o

The consistency of the presented observations with the well-known physical phenomena allows stressing the validity of the developed map conversion methods. Also, one must focus on the (ψ, ϕ, η_{is}) map as a powerful turbomachines' performance analysis tool. Actually, it is that formalism that makes it possible to quantify the compressibility effect, to extract kinematic information about the flow field - therefore about the turbomachine's geometry - and to enlighten off-design operating points.

Conclusions

The present study had undertaken the definition of analytical relationships between the different turbomachines' characterization maps, namely the compressor/turbine (π_c, MFP, η_{is}) map, the propeller (τ, J, χ) map and the (ψ, ϕ, η_{is}) map. The developed equations are bijective which makes it possible to convert any initial characteristic map into the other two in order to take advantage of each map. Actually, the (ψ, ϕ, η_{is}) map had been used to develop a mean flow features extraction method that determines the rotor outlet relative flow angle and the mean-streamline radius.

These relationships and the mean flow features extraction method had been applied to both turbofan's fan stage and a propeller which helped to highlight the powerful potential of the (ψ, ϕ, η_{is}) formalism as a performance analysis tool. Indeed, the physical analyses of the obtained results and comparisons to experiments allow drawing some important conclusions:

- The compressibility effects on the global performance parameters of an unchoked turbomachine are negligible while the variation of axial flow stays small (i.e. k factor close to unit).
- The rotor outlet relative flow angle at reference radius of a single-stage unchoked fan can be analytically derived from its characteristic map with an error up to 15%.
- The definition of the meridional mean-streamline of the flow in a single-stage unchoked fan can be obtained through the equation (5) as proposed by Binder [20].
- The geometry of the stream tube that defines the flow through a propeller can be analytically derived using the equation (32), both for design and off-design operating points.

- The design pitch angle of a propeller can be analytically derived through the extraction of the flow angles and the analysis of the resulting deviation angle.

These results, through their coherence with the physics of the studied turbomachines bring a first level of validation to the developed equations.

Finally, the developed methods allow the characterization of all axial turbomachines using the most unified tool that is the (ψ, ϕ, η_{is}) formalism. This map already showed its relevance in the unification of the turbomachines' treatment through its usage in the works of Gill et al. [17] and Binder et al. [18–20] on low-speed fans and radial turbines. This contribution adds turbofan's fan stages and propellers to the later list. In addition to this, it is important to stress the ability of the (ψ, ϕ, η_{is}) map to represent clearly the off-design operation of the turbomachine. In particular the blades pitch angle variation that opens very promising prospects for the analytical modelisation of this geometrical variability inside current system-oriented reasearch on innovative propulsive systems.

References

[1] European Commission. Flightpath 2050 Europe's Vision for Aviation. Technical report, European Union, 2011.

[2] U.S. Government. U.S. Aviation Greenhouse Gas Emissions Reduction Plan. Technical report, 2015.

[3] K. Zarati, S. Duplaa, X. Carbonneau, and N. Tantot. Engine performance and surge margins optimization by means of nozzles variability. In *22nd ISABE Conference*, Phoenix, AZ, 2015.

[4] A. Joksimović, S. Duplaa, Y. Bousquet, X. Carbonneau, and N. Tantot. Local and global analysis of a variable pitch fan turbofan engine. In *European Turbomachinery Conference*, Stockholm, 2017.

[5] IATA, DLR, and Georgia Tech. IATA Technology Roadmap. Technical report, IATA, 2013.

[6] D. Japikse and N. C. Baines. *Introduction to turbomachinery*. Concepts ETI, 1997.

[7] G. F. Wislicenus. *Fluid Mechanics of Turbomachinery*. McGraw-Hill, New-York, 1947.

[8] B. Lakshminarayana. *Fluid dynamics and heat transfer of turbomachinery*. Wiley, 1996.

[9] S. L. Dixon and C. A. Hall. *Fluid mechanics and thermodynamics of turbomachinery*. Butterworth-Heinemann, Waltham (MA), seventh edition, 2014.

[10] O. Cordier. Ähnlichkeitsbedingungen für Strömungsmaschinen. *Brennstoff Wärme Kraft Zeitschrift*, 10(5):337–340, 1953.

[11] O. E. Balje. *Turbomachines : a guide to design selection and theory*. Wiley, 1981.

[12] M. Casey, C. Zwyssig, and C. Robinson. The Cordier Line for Mixed Flow Compressors. In *ASME Conference Proceedings*, pages 1859–1869, Glasgow, 2010.

[13] P. Epple, F. Durst, and A. Delgado. A theoretical derivation of the Cordier diagram for turbomachines. In *Proceedings of the Institution of Mechanical Engineers, Part C: Journal of Mechanical Engineering Science*, volume 1, pages 1–15, 2010.

[14] R. I. Lewis. *Turbomachinery Performance Analysis*. Elsevier Science, 1996.

[15] R. T. Knapp, Pasadena, and Calif. Complete Characteristics of Centrifugal Pumps and Their Use in the Prediction of Transient Behavior. *A.S.M.E. Transactions*, (11), 1937.

[16] R. C. Turner and D. W. Sparkes. Complete characteristics for a single-stage axial flow fan. *Proceedings of the Institution of Mechanlical Engineers*, 178:14–27, 1963.

[17] A. Gill, T. W. Von Backström, and T. M. Harms. Fundamentals of four-quadrant axial flow compressor maps. *J. Power and Energy*, 221, 2007.

[18] N. Binder, S. Le Guyader, and X. Carbonneau. Analysis of the Variable Geometry Effect in Radial Turbines. *Journal of Turbomachinery*, 134(4), 2012.

[19] N. Binder, S.-K. Courty-Audren, S. Duplaa, G. Dufour, and X. Carbonneau. Theoretical Analysis of the Aerodynamics of Low-Speed Fans in Free and Load-Controlled Windmilling Operation. *Journal of Turbomachinery*, 137(10), 2015.

[20] N. Binder. *Aéro-thermodynamique des Turbomachines en Fonctionnement Hors-Adaptation*. Hdr thesis, ISAE-Supaero/DAEP, 2016.

[21] A. Carter. Low speed performance of related aerofoils in cascades. Technical report, 1950.

[22] N. García Rosa, G. Dufour, R. Barènes, and G. Lavergne. Experimental Analysis of the Global Performance and the Flow Through a High-Bypass Turbofan in Windmilling Conditions. *Journal of Turbomachinery*, 137(5):1–8, 2015.

[23] G. Dufour, N. Garcia Rosa, and S. Duplaa. Validation and flow structure analysis in a turbofan stage at windmill. *Proceedings of the Institution of Mechanical Engineers, Part A: Journal of Power and Energy*, 229(6):571–583, 2015.

[24] Pratt & Whitney Canada. Pratt & Whitney Canada. PW100/150. Visited on February 21st 2017. http://www.pwc.ca/en/engines/pw100-pw150.

[25] E. P. Hartman and D. Biermann. The aerodynamic characteristics of full-scale propellers having 2, 3, and 4 blades of clark Y and R.A.F. 6 airfoil sections. Technical report, NACA, 1937.

[26] B. W. McCormick. *Aerodynamics, aeronautics, and flight mechanics*. Wiley, New-York, second edition, 1995.